land

MDPI

*Article*

# Risk Assessment of Earthquake–Landslide Hazard Chain Based on CF-SVM and Newmark Model—Using Changbai Mountain as an Example

**Kai Ke [1], Yichen Zhang [1,*], Jiquan Zhang [2], Yanan Chen [1], Chenyang Wu [3], Zuoquan Nie [1] and Junnan Wu [1]**

[1] College of Jilin Emergency Management, Changchun Institute of Technology, Changchun 130012, China
[2] School of Environment, Northeast Normal University, Changchun 130117, China
[3] College of Surveying and Mapping Engineering, Changchun Institute of Technology, Changchun 130021, China
* Correspondence: zhangyc@ccit.edu.cn

**Abstract:** Changbai Mountain is an important part of the development and opening pilot area of Changjitu. It is the birthplace of Songhua River, Yalu River, and Tumen River, and is known as the source of the three rivers. Millions of people live in the basin. A volcanic eruption accompanied by earthquakes would lead to a large number of landslides, debris flows, and show a chain effect, the formation of a secondary geological disaster chain, which is a serious threat to people's lives and property safety. This paper selected indexes from three aspects: the hazard of earthquake-induced geological disaster chain, the exposure and vulnerability of disaster-bearing bodies, and the risk assessment of earthquake-induced geological disaster chain. The sensitivity values of each influence factor were calculated by the certainty factor (CF) using the support vector machine, and then, the susceptibility assessment was obtained. The cumulative displacement calculated by the Newmark model represented the potential risk intensity. We considered the Changbai Mountain volcanic earthquake–landslide disaster chain as an example. The results of risk assessment showed that the extremely high and high risk areas were mainly located within the 12 km radius of Tianchi Lake, and the other areas in the study area were mainly associated with very low to low risk values. The verification results showed that the receiver operating characteristic (ROC) curve area was 0.8373, indicating that the method was very effective in the identification and assessment of seismic hazard chain risk. In these high-risk areas, relevant countermeasures should be formulated to prevent the risk of geological disasters, strengthen the implementation of regional disaster prevention and reduction work, and ensure the safety of residents' lives and property.

**Keywords:** Changbai Mountain Nature Reserve; CF-SVM model; Newmark model; risk assessment



**Citation:** Ke, K.; Zhang, Y.; Zhang, J.; Chen, Y.; Wu, C.; Nie, Z.; Wu, J. Risk Assessment of Earthquake–Landslide Hazard Chain Based on CF-SVM and Newmark Model—Using Changbai Mountain as an Example. *Land* **2023**, *12*, 696. https://doi.org/10.3390/land12030696

Academic Editor: Deodato Tapete

Received: 13 February 2023
Revised: 8 March 2023
Accepted: 14 March 2023
Published: 16 March 2023



## 1. Introduction

The phenomenon of secondary disasters being caused by some kind of primary disaster is considered to be a disaster chain; the casualties and property damage related to disaster chains are deemed to be greater than those resulting from the primary source disasters themselves [1]. Therefore, disaster chain risk assessment became one of the urgent core issues to be addressed in current international research. Landslides, rockfalls, and debris flows are usually triggered by extreme rainfall or earthquakes [2,3]. In the geological disaster chain, a landslide caused by rainfall or an earthquake is one of the most dangerous geological disaster chains in mountainous areas and will cause a large number of casualties and significant economic losses [4–7]. Landslides are quite common and catastrophic in China, due to intense tectonic movements caused by the Himalayan orogeny. In 2016, more than 80 people died in the Xinmo landslide in Sichuan province [8,9]. Landslides caused by heavy rainfall in Su village, Zhejiang Province, killed 27 people [10]. In 2008, a devastating earthquake with a magnitude of 8.0 occurred in Wenchuan, Sichuan Province, China, which

triggered a series of disaster chains, such as the earthquake–landslide–reservoir disaster chain and earthquake–landslide–debris flow disaster chain, causing a total of 69,225 casualties [11,12]. In 2013, a 7.0 magnitude catastrophic earthquake occurred in Lushan, Sichuan Province, China, which triggered many landslides and caused a large number of casualties [13]. Nowadays, a large number of scholars in China and abroad have carried out much research on geological hazard chains and summarized a large number of methods, such as probability analysis based on data and risk assessment model construction through Bayesian network [14]. Research on disaster chain mechanism based on field investigation and remote sensing interpretation was conducted [15–17]. In addition, logistic regression, support vector machines, random forests, and neural network in machine learning and deep learning can be used to analyze the prone probability of a disaster chain [18–22]. A large number of numerical simulation models, such as Massflow, RAMMS-DEBRIS FLOW, and TRIGRS, were applied to predict disaster chains and analyze the formation mechanism by simulating the spatial distribution of landslides or debris flows initiated under the trigger of rainfall or other factors [23–26]. Li and Xue combined the certainty coefficient and the support vector machine to conduct susceptibility evaluation of geological disasters [26,27]. The finite element method, pseudo-static analysis, and Newmark are commonly used in secondary disasters caused by earthquakes [27–29]. By identifying potential areas of unstable slopes caused by earthquakes and calculating cumulative dislocations, the Newmark model evaluates the related hazard of the earthquake–landslide disaster chain [30–32]. Hazard assessment mainly includes two aspects: the spatial probability and the time probability of disaster occurrence. Spatial probability refers to what is likely to happen under the conditions of induced events, i.e., susceptibility. The time probability is the frequency or intensity of the inducing factor. In many articles, CF-SVM models were often used to assess the sensitivity of single hazards without considering the riskiness of hazard chains. Second, the CF-SVM model does not adequately reflect the nature of earthquake effects on secondary hazards, nor does it calculate the hazard intensity of earthquake hazards well. Based on the above deficiencies, this study proposed a volcanic earthquake–collapse–landslide disaster chain risk evaluation model on the basis of a CF-SVM model and the Newmark model. The risk evaluation model was constructed according to natural disaster risk formation theory from the perspective of the overall disaster chain. The CF-SVM model can be used to analyze the chain probability (susceptibility) between adjacent hazard events and to analyze the hazard intensity of earthquakes on secondary hazards based on the permanent displacement calculated from the Newmark model, because the permanent displacement obtained from the Newmark model can better describe the impact of earthquakes on secondary hazards. The effectiveness of this evaluation method was verified by using the seismic-landslide hazard chain caused by the volcanic eruption of Changbai Mountain as a case study. Through the earthquake hazard chain risk assessment model and case study, the chain probability of the hazard environment, the hazard intensity of the hazard factors, the vulnerability of the carrier, and the exposure of the carrier were considered on the basis of natural hazard risk theory. In this paper, the susceptibility between adjacent disaster events was obtained by combining the certainty coefficient and support vector machine, and the hazard intensity of earthquake to secondary disasters was analyzed according to the permanent displacement calculated by the Newmark model. The process of the comprehensive model of earthquake disaster chain risk identification is shown in Figure 1. The seismic and landslide disaster chain caused by the volcanic eruption on Changbai Mountain was taken as a case study to verify the effectiveness of the method.

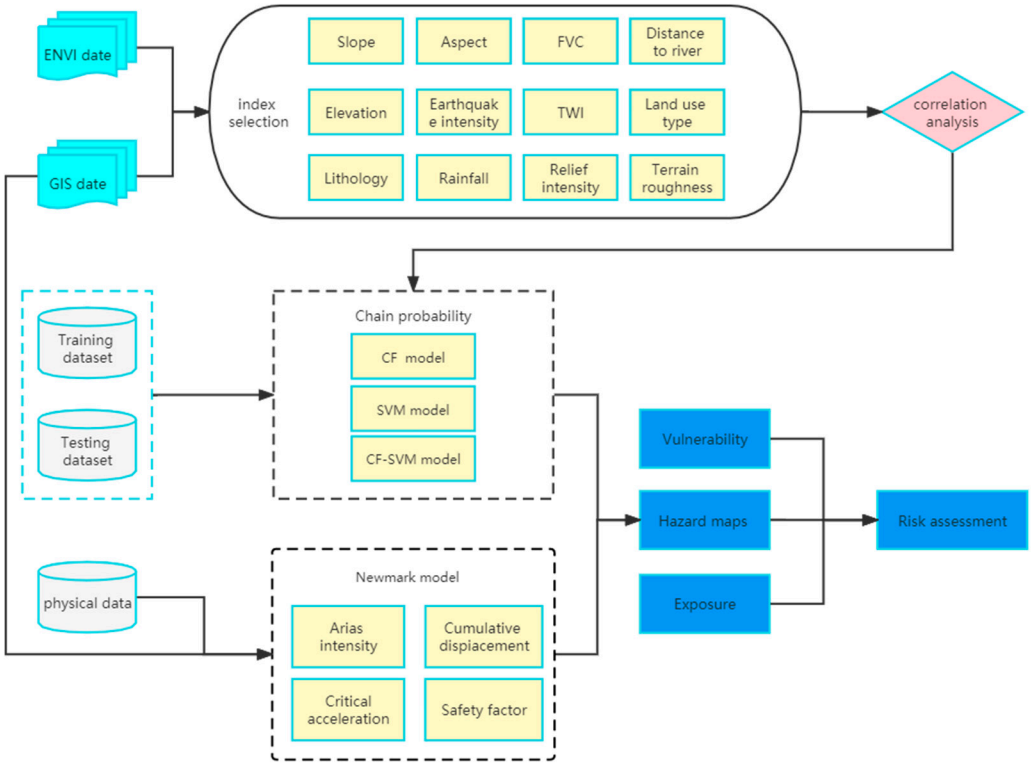


**Figure 1.** The risk assessment process of the earthquake disaster chain.

## 2. Study Area

The Changbai Mountain Protection and Development Zone is located in the southeastern mountainous area of Jilin Province. It is under the jurisdiction of the Management Committee of Changbai Mountain Protection and Development Zone of Jilin Province, covering an area of 3278 km$^2$. The geographical coordinates are 127°28′–128°16′ east longitude and 41°42′–42°25′ north latitude (Figure 2). The climate in Changbai Mountain is a semi-humid continental climate in the middle temperate zone. Due to the influence of terrain and continental and Pacific air currents, vertical zonation is obvious in this region. The temperature and precipitation are controlled by altitude. The region's climate is characterized by long and cold winters, warm and short summers, and slow and fleeting spring and autumn. The average annual precipitation is 1407.6 mm, and the precipitation is concentrated in June to August. The precipitation in three months accounts for more than 60% of the total annual precipitation, and most of it is heavy rain.

Changbai Mountain has a unique topographic and geomorphic landscape. The overall terrain is centered on the volcanic cone, which decreases sharply to the four sides. The top center of the cone is Tianchi Volcanic Lake, with an elevation of 2189.7 m above sea level. Due to the local fault movement, volcanic seismic activity showed an obvious upward trend since 2002. Due to the many eruptions in the history of Changbai Mountain, a large amount of pyroclastic deposits were distributed around the Tianchi Lake, especially on both sides of the Erdaobai River main gully. Changbai Mountain is a famous tourist area and national nature reserve, which attracts many tourists. More than 20,000 people (local residents and tourists) were affected by secondary disasters in the region. Due to the many historical eruptions of Changbai Mountain volcanoes, a large amount of volcanic debris accumulation was distributed around Tianchi, especially on both sides of the main gorge of the Erdao Bai River, and the soft rocks and loose accumulation were eroded by flowing water, the valley was undercut, and the front edge of the slopes on both sides of the river formed an open sliding space, and the volcanic earthquakes caused deformation of the mountain, and landslides occurred when the rock structure of the slope was damaged, which seriously threatened the safety of people's lives and properties [33].

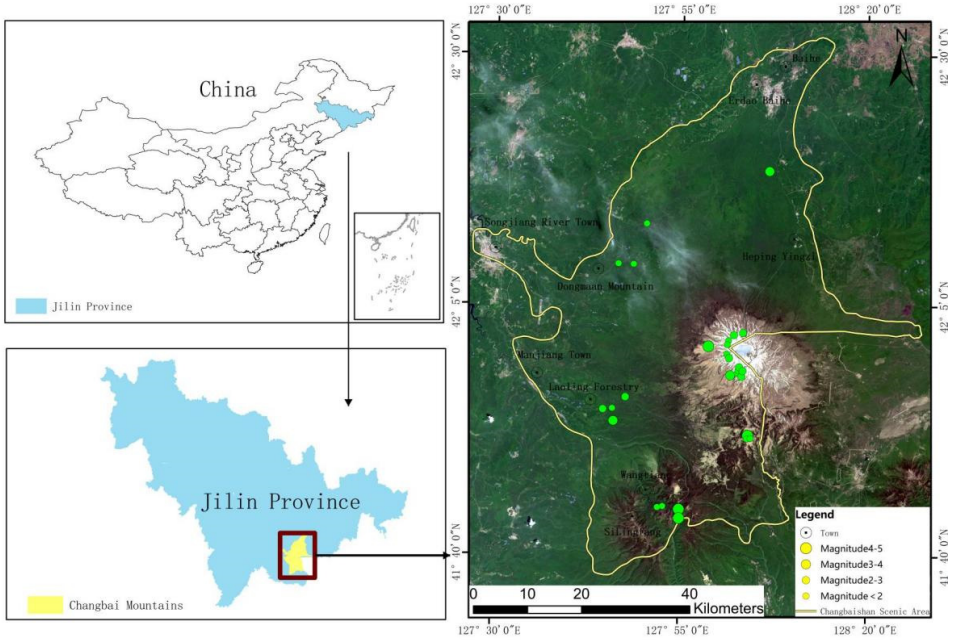


**Figure 2.** Location of the study area and distribution of seismic sites.

## 3. Data and Methods

### *3.1. Certainty Factor*

The certainty factor (CF) is essentially a probability function. It was first proposed by Shortliffe [34] and improved by Heckerman [35] for analyzing the sensitivity of various factors affecting the occurrence of certain event [36]. Based on existing debris flow disaster events, and assuming that the conditions of future debris flow disasters are the same as those that have occurred, the contribution degrees of different sections or categories within each impact factor were calculated. The CF model can analyze the sensitivity of debris flow disaster factors and complete the susceptibility evaluation of debris flow disaster. The calculation formula is:

$$CF = \begin{cases} \frac{PP_a - PP_s}{PP_a(1-PP_s)} & PP_a \geq PP_s \\ \frac{PP_a - PP_s}{PP_s(1-PP_a)} & PP_s \geq PP_a \end{cases} \quad (1)$$

where CF is the certainty factor of debris flow disaster occurrence, $pp_a$ is the ratio of debris flow disaster area in evaluation factor a to the area occupied by evaluation factor a, a is a certain level in any indicator; $pp_s$ is the prior probability of debris flow disaster occurring in the whole study area, specifically represented by the ratio of the total area of debris flow disaster in the whole study area to the total area of the study area. The CF value calculated based on the above formula is −1–1, and the calculated result is regular, indicating that this unit is the prone area of debris flow disaster. Otherwise, if the calculated result is negative, it means that debris flow disaster is not easy to occur in this unit. Soil properties and faults have important effects on earthquake-induced landslides, but the data obtained are difficult to obtain because of the small distribution of faults in the study area and their distribution in the boundary areas. Therefore, fault and soil indicators were not added. Slope, aspect, relief intensity, lithology, elevation, topographic wetness index (TWI), earthquake intensity (EI), rainfall, fractional vegetation cover (FVC), land use type (LUT), distance to river (DTR), and terrain roughness(TR) were selected as evaluation indexes to obtain the susceptibility index and normalize it into the spatial probability of earthquake-debris flow chain. The data sources are shown in Table 1. Indicators are selected as shown in Figure 3.

**Table 1.** Data source.

| Evaluation Index | Data Type | Resolution | Data Source |
|---|---|---|---|
| Elevation | raster data | 30 m | Geospatial data cloud |
| Land use type | raster data | 30 m | National Center for Basic Geographic Information |
| Rainfall | raster data | 30 m | National Data Center for Meteorological Sciences |
| Fractional vegetation cover | Landsat 8 OLI/TIRS | 30 m | Satellite remote sensing cloud for natural resources |
| Slope | raster data | 30 m | Geospatial data cloud |
| Distance to river | vector data | 30 m | Geospatial data cloud |
| Aspect | raster data | 30 m | Geospatial data cloud |
| Lithology | vector data | 30 m | Geological cloud |
| Relief intensity | vector data | 30 m | Geospatial data cloud |
| Topographic wetness index | vector data | 30 m | Resources and Environmental Sciences and Data Center, Chinese Academy of Sciences |
| Earthquake intensity | raster data | 30 m | Google earth pro |
| Terrain roughness | vector data | 30 m | Resources and Environmental Sciences and Data Center, Chinese Academy of Sciences |
| Population | vector data | 30 m | Resources and Environmental Sciences and Data Center, Chinese Academy of Sciences |
| Gross national product | vector data | 30 m | Resources and Environmental Sciences and Data Center, Chinese Academy of Sciences |
| Building density | vector data | 30 m | National Center for Basic Geographic Information |
| Road density | vector data | 30 m | National Center for Basic Geographic Information |
| Age level | vector data | 30 m | Resources and Environmental Sciences and Data Center, Chinese Academy of Sciences |

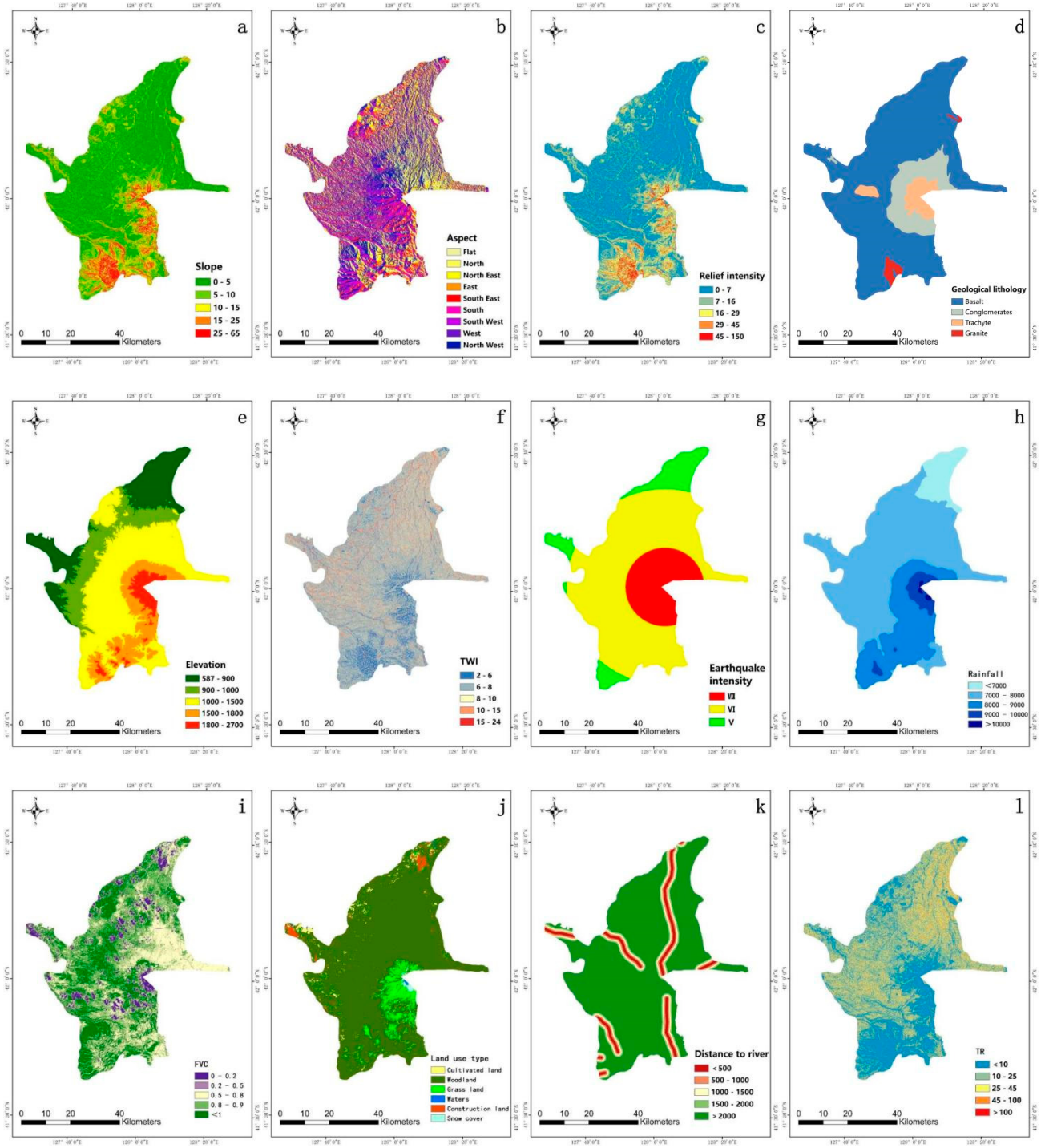


**Figure 3.** Condition parameters: (**a**) slope, (**b**) aspect, (**c**) relief intensity(RI), (**d**) lithology, (**e**) elevation, (**f**) topographic wetness index (TWI), (**g**) earthquake intensity (EI), (**h**) rainfall, (**i**) fractional vegetation cover (FVC), (**j**) land use type (LUT), (**k**) distance to river (DTR), (**l**) terrain roughness (TR).

### *3.2. Support Vector Machine (SVM)*

Based on the theory of machine learning, support vector machines (SVMS) were first proposed by VAPNIK in the 1960s when studying small samples [37]. They are considered to be the best theory for small sample estimation and predictive learning at present and are widely used in disaster sensitivity assessment [38]. The classification of data points can be realized by calculating the distance between the data points and the hyperplane, and the reliability of the result is positively correlated with the distance. In the case of

fewer samples, the low-dimensional nonlinear data can be mapped to the high-dimensional space, and the optimal hyperplane can be used to separate the two types of data and ensure the maximum separation interval [39,40]. Taking the binary classification problem as an example, the training sample is assumed to be ($x_i$, $y_i$), $x_i \in x^n$, $y_i \in Y$, Where I = (1,2,3, . . . , l), n is the eigenspace of sample X, $y_i = \pm 1$. The goal of SVM is to find a hyperplane with n-dimensional feature space and w normal vector, namely $W^T X + b = 0$, separating the two types of data points correctly, while keeping the classification spacing as wide as possible. In order to meet the above classification requirements, this problem can be converted into a minimum value problem with constraints [41]:

$$min\ \frac{1}{2}\|w\|^2 \tag{2}$$

$$s.t.\ y_i\left(w^T x_i + b\right) \geq 1, \qquad i = 1, 2, \ldots, m$$

This problem can be converted into a convex quadratic programming problem. In the case of linear indivisibility, by introducing a relaxation variable $\xi_i \geq 0$ and penalty factor C, the convex quadratic programming problem becomes:

$$min\ \frac{1}{2}\|w\|^2 + C\sum_{i=0}^{m} \xi_i \tag{3}$$

$$s.t.\ y_i\left(w^T x_i + b\right) \geq 1 - \xi, \qquad i = 1, 2, \ldots, m$$

In the formula (3), C > 0 is a constant, and its size determines the punishment degree of wrong sampling.

The model is convex quadratic programming (global extremum of local extremum and quadratic constraint of objective function). It can be solved directly with the existing optimization package, but there can be a more efficient method. Using the Lagrange multiplier method, the optimization problem of two parameters is transformed into one parameter optimization problem, and then the model is solved. The Lagrange multiplier method is used to transform the constraints into objective functions, that is, Lagrange multiplier $\alpha_I > 0$ is added to each constraint. The Lagrange function is obtained as follows [42]:

$$L(w, b, \alpha) = \frac{1}{2}\|w\|^2 + \sum_{i=1}^{m} \alpha_i\left(1 - y_i\left(w^T x_i + b\right)\right) \tag{4}$$

Solving Equation (4) yields the optimal classification function:

$$w^T x + b = \left(\sum_{i=1}^{m} \alpha_i y_i x_i\right)^T x + b = \sum_{i=1}^{m} \alpha_i y_i \langle x_i, x\rangle + b \tag{5}$$

SVM uses kernel functions to solve nonlinear classification problems. At present, the commonly used kernel functions of SVM mainly include linear kernel, polynomial kernel, radial basis kernel, and Sigmoid kernel function. Radial basis kernel function is widely used in disaster sensitivity evaluations [43], but for different research purposes, the prediction accuracy of four kernel functions should be compared, and the optimal kernel function should be selected to establish a SVM prediction model.

### *3.3. Newmark Model*

The theoretical basis of the Newmark model is the limit equilibrium theory. It is considered that the permanent deformation of the slider is caused by the destruction of the block along the sliding surface under the seismic load. When the acceleration applied at the sliding surface exceeds the critical acceleration in its limiting equilibrium state, the block slides along the destruction surface, that is, the slide is not displaced when the seismic acceleration value is less than the critical acceleration $a_c$, the displacement of the slider is generated by a fraction greater than the critical acceleration [44], quadratic integration of the difference between the load acceleration $a_t$ and the critical acceleration $a_c$ yields the

cumulative shift value $D_N$. Jibson, using 2270 strong vibration records from 30 earthquakes around the world, established an empirical model with the critical acceleration $a_c$ and Arias intensity $I_a$ as the parameters. The formula was described as follows [45]:

$$logD_N = 2.401logI_a - 3.481loga_c - 3.230 \pm 0.656 \quad (6)$$

Arias intensity is a physical measure of the total intensity of the ground motion and refers to the sum of the squares of the vibration acceleration recorded by the instrument, expressed by $I_a$, in $m{\cdot}s^{-1}$. Wilsongave the empirical formula of the value based on 43 seismic records [46]:

$$I_a = 0.9T(a_{max})^2 \quad (7)$$

where $a_{max}$ is the seismic peak acceleration; T is the Dobre duration, the expression is $lgT = 0.432M - 1.83$, and M is the seismic magnitude calculated at the Richter scale. According to the seismic intensity attenuation formula, the seismic intensity I corresponding to different epicenter distances r can be obtained in eastern China:

$$I = 4.493 + 1.454M - 1.792ln(r + 16) \quad (8)$$

$a_{max}$'s relationship to the seismic intensity formula can be expressed as [47]:

$$I = 3.322log(a_{max}) + 0.033 \quad (9)$$

In combination with formulas (8) and (9), the grid data files of PGA parameters of the study area were generated in Arc GIS software, and the results of the calculation were replaced into formula (7).

The calculation of the critical acceleration $a_c$ is usually based on the comparison of the static conditions of the slide and the seismic dynamic conditions, using the infinite slope method, namely [48]:

$$a_c = (F_s - 1)g\ sin\ \alpha \quad (10)$$

where $\alpha$ is the slope foot; the expression for $F_s$ is as follows:

$$F_s = \frac{c}{\gamma h \sin\alpha} + \frac{\tan\varphi}{\tan\alpha} - \frac{m\gamma_w \tan\varphi}{\gamma \tan\alpha} \quad (11)$$

$\varphi$ is the internal friction angle (°); c is the cohesion force (kPa); $\gamma$ is the geotechnical body mass degree ($N{\cdot}m^{-3}$); $\gamma_w$ is the severity of water ($N{\cdot}m^{-3}$); $h$ is a slider thickness (m); and m is the ratio of the thickness of the slide immersed in water to the slide thickness. The parameter values for these rock masses are listed in Table 2.

**Table 2.** Classification of engineering rock mass grade and its parameter value (GB50218T-2014, China).

| Rock Group | c/Mpa | φ/(°) | γ $(kN/m^3)$ |
|---|---|---|---|
| Hard rock | >0.22 | >37 | >26.5 |
| Second hard rock | 0.12–0.22 | 29–37 | >26.5 |
| Second soft rock | 0.08–0.12 | 19–29 | 24.5–26.5 |

### *3.4. Risk Assessment Model of Earthquake-Induced Landslide Disaster Chain*

In this study, hazard and vulnerability were considered in the earthquake disaster chain risk evaluation model. We defined hazard as the influence of the activity scale, and the frequency of the hazard factors on the disaster body. Disaster chain hazard analyses included a susceptibility analysis of the disaster chain (chain probability) and a hazard

intensity analysis of the disaster chain (the sum of the hazard intensities of each disaster event). Combining the sensitivity results, the hazard was calculated using Equation (12).

$$H = S \times C \tag{12}$$

where H is the hazard value of disaster chain, H is the hazard of disaster chain, S is the susceptibility, and C is the hazard intensity.

According to the formation mechanism of natural disaster risk, the natural disaster risk index method was used to establish the risk degree. The specific calculation formula is as follows:

$$R = H^{W_h} \times V^{W_v} \times E^{W_e} \tag{13}$$

Formula: R is the risk index of earthquake-induced landslide disaster chain, the greater the value represents the greater the disaster risk; the values of H, V, E indicate the hazard, vulnerability, and exposure of earthquake-induced landslide disaster chain, respectively; $W_h$, $W_v$, and $W_e$ are the weights of each factor, which were calculated by the variation coefficient method as 0.1549, 0.4149, and 0.4302.

## 4. Geological Hazard Susceptibility Assessment Results

### *4.1. Correlation Analysis of Evaluation Factors*

When selecting evaluation factors to evaluate the vulnerability of geological disasters, each evaluation factor may have a correlation, but the evaluation factor with high correlation is often not representative, resulting in redundancy of the evaluation factors, which affects the accuracy of the evaluation model, which is likely to affect the accuracy of the evaluation results. Based on this, the Pearson correlation coefficient method was used to analyze the correlation of each evaluation factor, and the evaluation factors with high correlation were eliminated, while those with no correlation or low correlation were retained. The Pearson correlation coefficient method is a statistical method used to express the degree of correlation between several variables, which is usually expressed by r. The size of r represents the degree of correlation of factors. The larger the value of r, the higher the degree of correlation. The solution formula is as follows:

$$r = \frac{\sum_{i=1}^{n}(x_i - \overline{x})(y_i - \overline{y})}{\sqrt{\sum_{i=1}^{n}(x_i - \overline{x})^2}\sqrt{\sum_{i=1}^{n}(y_i - \overline{y})^2}} \tag{14}$$

In the formula, n represents the number of samples, $x_i$ and $y_i$ represent the observed values of sample variables, and $\overline{x}$ and $\overline{y}$ represent the mean values of samples.

The degree of linear relationship between two variables is generally described by the correlation coefficient r, $|r| > 0.95$ represents a significant correlation, $|r| \geq 0.8$ represents a high correlation, $0.5 \leq |r| < 0.8$ represents a moderate correlation, $0.3 \leq |r| < 0.5$ represents a low correlation, $|r| < 0.3$ represents an extremely weak, which was considered irrelevant. P is the probability of significance, $p > 0.05$ indicates no significant difference; $0.01 < p < 0.05$ indicates that the correlation is significant and is marked with * in the figure; $p < 0.01$ indicates a significant correlation, marked with ** in the figure. The blue section of the figure indicates positive correlation, and the red section indicates negative correlation. From Figure 4, the correlation coefficient between slope and topographic fluctuation was 0.99 positive correlation, with high correlation, and $p < 0.01$ significant difference; the correlation coefficient between elevation and rainfall was 0.95 positive correlation, with high correlation, and $p < 0.01$ significant difference. As seen in Figure 4, the remaining factors were medium or low degree correlation, or basically unrelated. Slope and annual average rainfall are important indicators to evaluate earthquake and landslide geological disasters, and so, the relief intensity and elevation were eliminated. Finally, 10 evaluation factors affecting the development of earthquake and landslide geological disasters in Changbai Mountain were determined.

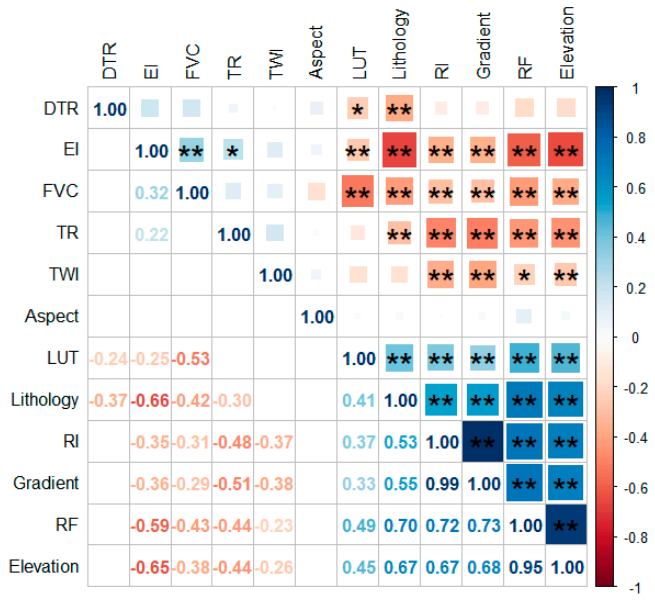


**Figure 4.** Correlation analysis chart of susceptibility indicators.

### *4.2. Susceptibility Assessment Based on CF-SVM*

The basic idea of using the CF-SVM model to evaluate the vulnerability of geological disasters is: the sensitivity values of each influence factor calculated by the CF method (Table 3) are taken as the classification data of the SVM model, and the training data is used to train the SVM, to realize the vulnerability evaluation of geological disasters in the whole study area. According to the known geological disaster hidden danger units, the downsampling method is used to cluster the non-geological disaster hidden danger units. At the clustering center, the number of units consistent with the number of geological disaster hidden danger units are selected as the non-geological disaster hidden danger units, and the two parts of data are taken as the sample data. A total of 104 landslide points and non-landslide points were generated in the study area, and the values of the four risk zoning maps after reclassification were extracted into the attributes of these 104 disaster points in ArcGIS as sample data. In the sample data, 70% of cells were randomly selected as training data and 30% of cells were randomly selected as validation data. The radial basis function was selected as SVM kernel function. The optimal parameter combination was determined by the cross validation method, and the optimal SVM model was established to predict the whole study area. The geological hazard susceptibility index of the study area was calculated, and then, the natural discontinuity method was adopted to divide the whole study into five susceptibility intervals: extremely high susceptibility area, high susceptibility area, medium susceptibility area, low susceptibility area, and very low susceptibility area. The geological hazard susceptibility zoning table and geological disaster susceptibility zoning map were obtained.

**Table 3.** Certainty Factor.

| Evaluation Index | Grade | Grading Area Ratio | Disaster Point Ratio | $PP_a$ | $PP_s(1-PP_a)$ | CF | Frequency Ratio |
|---|---|---|---|---|---|---|---|
| Slope/(°) | 0–5 | 0.5677 | 0.2692 | 0.0075 | 0.0073 | −0.5297 | 0.4742 |
| | 5–10 | 0.2531 | 0.1923 | 0.0120 | 0.0118 | −0.2432 | 0.7596 |
| | 10–15 | 0.0758 | 0.0769 | 0.0160 | — | 0.0145 | 1.0144 |
| | 15–25 | 0.0695 | 0.2115 | 0.0481 | — | 0.6820 | 3.0420 |
| | 25–65 | 0.0337 | 0.25 | 0.1173 | — | 0.8789 | 7.4085 |

**Table 3.** *Cont.*

| Evaluation Index | Grade | Grading Area Ratio | Disaster Point Ratio | $PP_a$ | $PP_s(1-PP_a)$ | CF | Frequency Ratio |
|---|---|---|---|---|---|---|---|
| aspect/(°) | −1–0 | 0.1142 | 0.0576 | 0.0079 | 0.0157 | −0.4990 | 0.5049 |
| | 0–22.5 | 0.1043 | 0.0961 | 0.0145 | 0.0156 | −0.0799 | 0.9211 |
| | 22.5–67.5 | 0.0854 | 0.0961 | 0.0178 | — | 0.1131 | 1.1253 |
| | 67.5–112.5 | 0.0680 | 0.0192 | 0.0044 | 0.0157 | −0.7204 | 0.2827 |
| | 112.5–157.5 | 0.0655 | 0 | 0 | 0.0158 | −1 | 0 |
| | 157.5–202.5 | 0.0942 | 0.0192 | 0.0032 | 0.0157 | −0.7986 | 0.2039 |
| | 202.5–247.5 | 0.1108 | 0.1730 | 0.0247 | — | 0.3653 | 1.5614 |
| | 247.5–292.5 | 0.1205 | 0.1730 | 0.0227 | — | 0.3081 | 1.4353 |
| | 292.5–337.5 | 0.1189 | 0.1730 | 0.0230 | — | 0.3180 | 1.4556 |
| | 337.5–360.0 | 0.1177 | 0.1923 | 0.0258 | — | 0.3938 | 1.6329 |
| Topographic wetness index (TWI) | 2.8–6 | 0.1415 | 0.2692 | 0.0301 | — | 0.4819 | 1.9022 |
| | 6–8 | 0.5565 | 0.4807 | 0.0136 | 0.0156 | −0.1380 | 0.8638 |
| | 8–10 | 0.1632 | 0.1538 | 0.0149 | 0.0156 | −0.0584 | 0.9424 |
| | 10–15 | 0.1205 | 0.0961 | 0.0126 | 0.0156 | −0.2050 | 0.7975 |
| | 15–24 | 0.0181 | 0 | 0 | 0.0158 | −1 | 0 |
| Fractional vegetation cover (FVC) | 0.0–0.2 | 0.0638 | 0.1923 | 0.0475 | — | 0.6774 | 3.0106 |
| | 0.2–0.5 | 0.0273 | 0.0769 | 0.0443 | — | 0.6534 | 2.8109 |
| | 0.5–0.8 | 0.2822 | 0.2307 | 0.0129 | 0.0156 | −0.1874 | 0.8176 |
| | 0.8–0.9 | 0.3090 | 0.2884 | 0.0147 | 0.0156 | −0.0708 | 0.9332 |
| | 0.9–1.0 | 0.3174 | 0.2115 | 0.0105 | 0.0156 | −0.3393 | 0.6664 |
| Rainfall/(mm) | <7000 | 0.0840 | 0 | 0 | 0.012456035 | −1 | 0 |
| | 7000–8000 | 0.6276 | 0.1923 | 0.0038 | 0.012408498 | −0.6962 | 0.3063 |
| | 8000–9000 | 0.2461 | 0.5384 | 0.0272 | — | 0.5497 | 2.1879 |
| | 9000–10000 | 0.0387 | 0.2115 | 0.0680 | — | 0.8272 | 5.4625 |
| | >10000 | 0.0034 | 0.0576 | 0.2069 | — | 0.9516 | 16.6164 |
| Land use type | Cultivated land | 0.0139 | 0 | 0 | 0.0158 | −1 | 0 |
| | Wood land | 0.8906 | 0.8269 | 0.0146 | 0.0156 | −0.0755 | 0.9284 |
| | Grass land | 0.0757 | 0.0961 | 0.0200 | — | 0.2128 | 1.2690 |
| | Waters | 0.0017 | 0 | 0 | 0.0158 | −1 | 0 |
| | Construction land | 0.0145 | 0 | 0 | 0.0158 | −1 | 0 |
| | Snow cover | 0.0033 | 0.0769 | 0.3637 | — | 0.9718 | 23.0417 |
| Lithology | Basalt | 0.7952 | 0.6538 | 0.0129 | 0.0156 | −0.1828 | 0.8221 |
| | Glutenite | 0.1336 | 0.0769 | 0.0090 | 0.0156 | −0.4300 | 0.5757 |
| | Trachyte | 0.0552 | 0.25 | 0.0714 | — | 0.7907 | 4.5235 |
| | Granite | 0.0158 | 0.0192 | 0.0191 | — | 0.1765 | 1.2141 |
| Earthquake intensity | VII | 0.1871 | 0.3269 | 0.0275 | — | 0.4326 | 1.7472 |
| | VI | 0.6868 | 0.6730 | 0.0154 | 0.0155 | −0.0236 | 0.9798 |
| | V | 0.1260 | 0 | 0 | 0.0158 | −1 | 0 |

**Table 3.** *Cont.*

| Evaluation Index | Grade | Grading Area Ratio | Disaster Point Ratio | $PP_a$ | $PP_s(1-PP_a)$ | CF | Frequency Ratio |
|---|---|---|---|---|---|---|---|
| Distance to river/(m) | <500 | 0.0461 | 0.0192 | 0.0071 | 0.0168 | −0.5878 | 0.4162 |
| | 500–1000 | 0.0473 | 0 | 0 | 0.0169 | −1 | 0 |
| | 1000–1500 | 0.0488 | 0.0192 | 0.0066 | 0.0168 | −0.6101 | 0.3939 |
| | 1500–2000 | 0.0499 | 0.0192 | 0.0065 | 0.0168 | −0.6189 | 0.3851 |
| | >2000 | 0.8076 | 0.9423 | 0.0197 | — | 0.1453 | 1.1666 |
| Terrain roughness | <10 | 0.3686 | 0.7115 | 0.0306 | — | 0.4896 | 1.9298 |
| | 10–25 | 0.4202 | 0.2692 | 0.0101 | 0.0157 | −0.3630 | 0.6406 |
| | 25–45 | 0.1399 | 0 | 0 | 0.0159 | −1 | 0 |
| | 45–100 | 0.0586 | 0.0192 | 0.0052 | 0.0158 | −0.675 | 0.3277 |
| | >100 | 0.0124 | 0 | 0 | 0.0159 | −1 | 0 |

As can be seen from Table 4, from the very low frequency area to the very high frequency area, the combined frequency ratio of the extremely high and high prone areas reached 82.49% of the total frequency ratio, which indicates that the deterministic coefficient (CF) model was also effective and feasible to evaluate the probability of geological disasters in Changbai Mountain. As seen in Figure 5, the sum of the geological disaster area in the red very high prone area and the orange high prone area accounted for 20.49% of the total area, the area ratio in the yellow middle prone area was 12.78%, and the area in the green low prone area and very low prone area was 66.73%. When the frequency ratio is >1, it indicates that this factor had a positive effect on landslide development, and that the frequency ratio had a greater influence [49]. The Fr method assumes that areas with similar geological conditions have a similar probability of geological disasters. The Fr value can quantitatively represent the relative degree of the influence of environmental factors on the occurrence of geological disasters [50]. An Fr value greater than 1 indicates that the environmental factor attribute interval is beneficial to the development of geological disasters, and the greater the value, the greater the impact on the development As seen in Table 4, when the susceptibility of CF evaluation model increased from low to high, the frequency ratio gradually increased, which is in line with the evaluation law. When the frequency ratio is greater than 1, the probability of geological disasters gradually increases.

**Table 4.** Statistical table of prone zoning.

| Model | Susceptibility | Division Area/km$^2$ | Area Proportion/% | Disaster Point | Disaster Point Ratio/% | Fr |
|---|---|---|---|---|---|---|
| CF-SVM | Very low | 1505.52 | 45.85 | 4 | 7.69 | 0.17 |
| | Low | 685.73 | 20.88 | 6 | 11.54 | 0.55 |
| | Moderation | 419.76 | 12.78 | 4 | 7.69 | 0.60 |
| | High | 175.21 | 5.34 | 6 | 11.54 | 2.16 |
| | Very high | 497.23 | 15.15 | 32 | 61.54 | 4.06 |

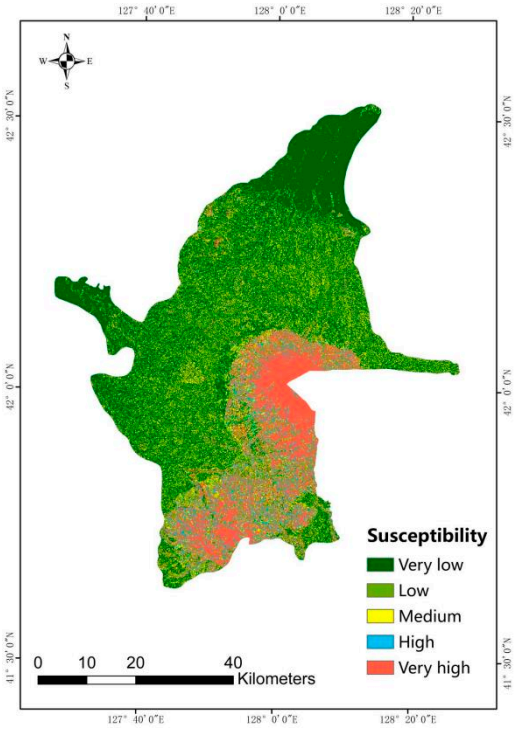


**Figure 5.** Earthquake-induced landslide susceptibility map.

### *4.3. Earthquake Intensity*

Due to a lack of data, Arias intensities for the entire study area must be obtained indirectly from seismic parameters. In 1991, Mount Pinatubo erupted with an earthquake magnitude of 5.6, which was the largest volcano-related earthquake magnitude recorded globally [51]. Based on this, a 6.0 magnitude earthquake can be predicted for the hypothetical eruption of Changbai Mountain volcano. According to Equation (6), the cumulative displacement of the Newmark model can be obtained (Figure 6).

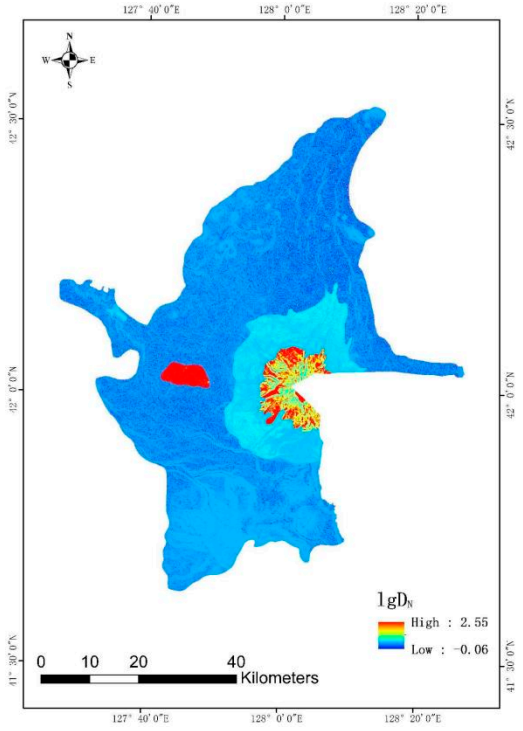


**Figure 6.** Cumulative displacement.

## 5. Risk Assessment

### *5.1. Hazard Assessment*

In view of the induced conditions of the seismically induced geological disaster chain, the cumulative displacement calculated according to the Newmark model was used as the index of the induced factor intensity of the seismically induced geological disaster chain. Combining the sensitivity results, the hazard was calculated using Equation (12). The calculated results were graded by natural breakpoint method to complete the hazard assessment of earthquake-induced landslide chain (Figure 7).

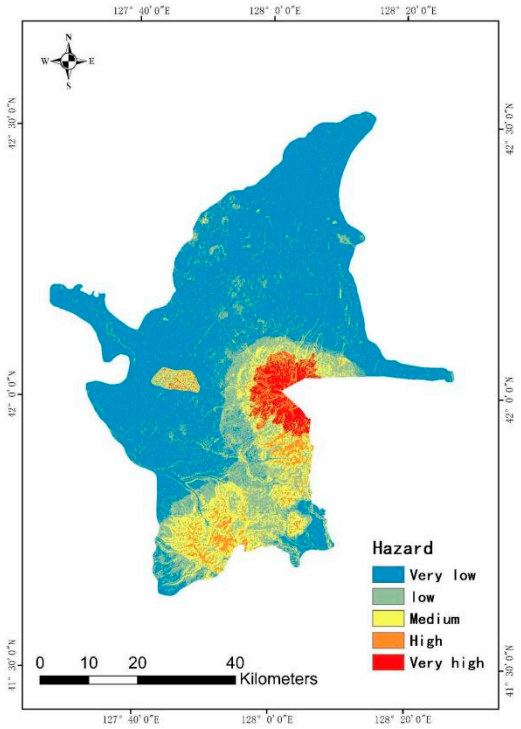


**Figure 7.** Earthquake-induced landslide hazard map.

### *5.2. Carrier Exposure Assessment*

The exposure of disaster-bearing body is a potential threat to the economic, social, and natural environment systems, especially the agricultural, human, and ecological environments. The basic work of the exposure assessment of a disaster-bearing body is the selection of the index and the determination of the weight of the assessment, as well as the modeling and evaluation of the disaster-bearing body exposure assessment. In this paper, the variation coefficient method was used to calculate the weights of various factors, and it was integrated with the method of a comprehensive weighted evaluation model to construct and evaluate the exposure evaluation model of a geological disaster-bearing body. The exposure evaluation index system and weight coefficient of the earthquake-induced slope disaster-chain-bearing body are shown in Table 5.

**Table 5.** Exposure evaluation index system and weight coefficient of disaster-bearing body.

| Primary Factor | Index | Weight Coefficient |
|---|---|---|
| Demographic factor | population | 0.2272 |
| Ecological environment factors | land use type | 0.2421 |
| Socioeconomic factor | gross national product | 0.5307 |

The exposure result of the disaster-bearing body was obtained by weighted superposition after quantization of indicators, and the classification was carried out by the natural

breakpoint method. Finally, the exposure zoning map was obtained (Figure 8). The overall exposure of disaster-bearing bodies in the study area was low. As for the Chinan District of Changbai Mountain, its land and economic exposure were relatively high, and the extremely exposed areas were generally distributed here. The high-exposure areas were mainly located in the Chixi District with moderate population and rapid economic development, while the medium-exposure areas were mainly located in the Chibei District with frequent human activities, and a few were located in the Chinan District. The low-exposure and extremely low-exposure areas were located in some areas with fewer people and lower economy in Chixi District and Chibei District.

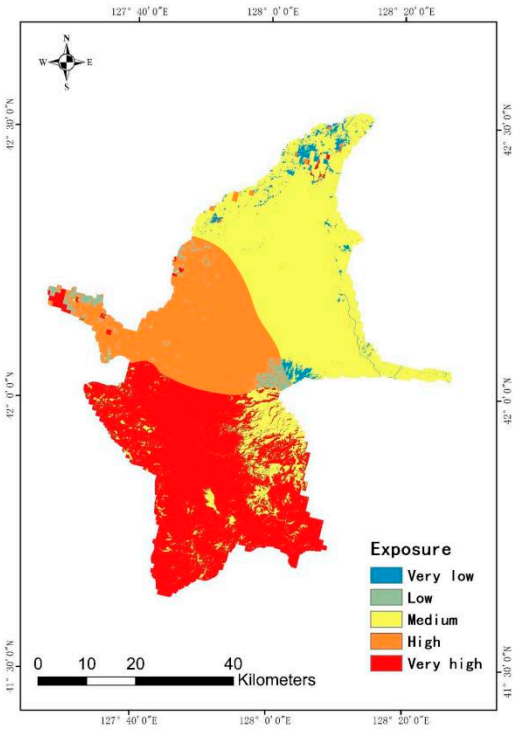


**Figure 8.** Earthquake landslide disaster exposure maps.

### *5.3. Carrier Vulnerability Assessment*

The vulnerability of a disaster-bearing body refers to the damage or damage scope suffered by a disaster-bearing body in a specific area, which, as a whole, reflects the damage (vulnerability) scope of disaster. Vulnerability is the loss caused by the value level of the recipient, including human casualties, economic losses, and loss of natural resources. It can be observed from the definition of vulnerability of a disaster-bearing body that the vulnerability of a disaster-bearing body refers to the material composition, structure, and state of the disaster-bearing body. At the same time, the main body affected by disasters includes natural factors and social economic factors. In this study, the variation coefficient method was used to calculate the weights of each index in the vulnerability assessment index system of the disaster-bearing body (Table 6), and the calculated results were combined with the vulnerability assessment model of the disaster-bearing body established according to the comprehensive weighted evaluation model to carry out the vulnerability assessment of the earthquake-induced landslide disaster chain (Figure 9).

**Table 6.** Disaster-bearing body vulnerability assessment index system and weight coefficient.

| Primary Factor | Index | Weight Coefficient |
|---|---|---|
| Demographic factor | Building density | 0.4856 |
| Ecological environment factors | Road density | 0.1690 |
| Socioeconomic factor | Age level | 0.3454 |

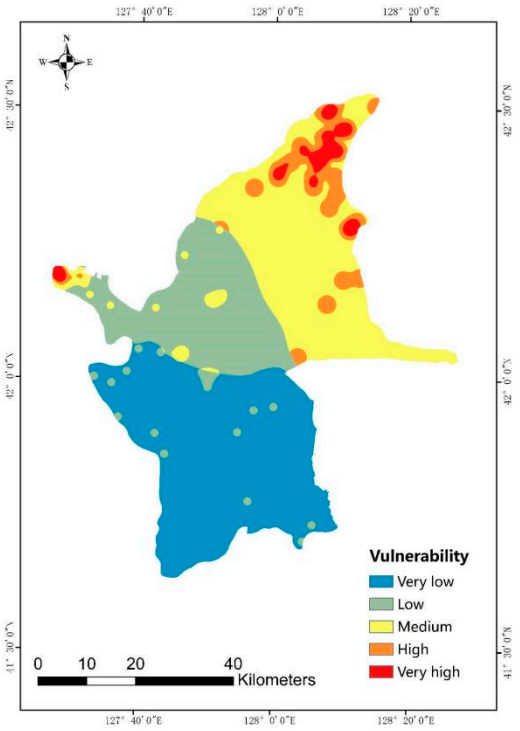


**Figure 9.** Earthquake landslide disaster vulnerability maps.

### *5.4. Results*

According to Equation (13) and the weight values, the risk index of the earthquake–landslide hazard chain was calculated and classified into five risk classes, including very low risk zone, low risk zone, medium risk zone, high risk zone, and very high risk zone, using the natural breakpoint method, and a risk zoning map was drawn (Figure 10).

Figure 10 shows the earthquake-landslide disaster chain risk zoning map that was constructed according to the disaster chain risk assessment model. From visual analysis of the earthquake disaster chain hazard map, it seemed to fit the trend of rainfall and slope. According to the area statistics in Figure 10, other regions in the study area mainly had very low or low risk values. The extremely high risk area accounted for 21% of the total area, the medium risk area accounted for 38%, and the low and very low risk area accounted for 41% of the total area. Overall, the high and medium risk areas were mainly located within 12 km radius of Tianchi Lake, which was strongly affected by volcanic activity. Other regions had low and very low risk values. Through the analysis of the seismic hazard chain hazard area, it was clear that the spatial trend of the seismic hazard chain hazard area followed the distribution of elevation and rainfall. Through the analysis of the seismic hazard chain hazard area, it was evident that the spatial trend of the seismic hazard chain hazard area followed the distribution of elevation and rainfall. More importantly, regarding the development of the hazard chain, the favorable terrain for earthquake-induced landslides was found to be high slope, and its change directly lead to the change of the surrounding disaster environment, greatly increasing the probability of landslide occurrence. The southern study area was less high-risk than the vicinity of Tien Chi, despite the high steep terrain, which was probably due to the lower average annual precipitation in the

area compared to the center of Tien Chi. The rainfall limited the occurrence of landslides; thus, the influence of the distance of rivers in the study area was not important. The risk assessment model of earthquake disaster chain proposed in this study provided a reference for the prevention of and reduction in the mountain disaster chain.

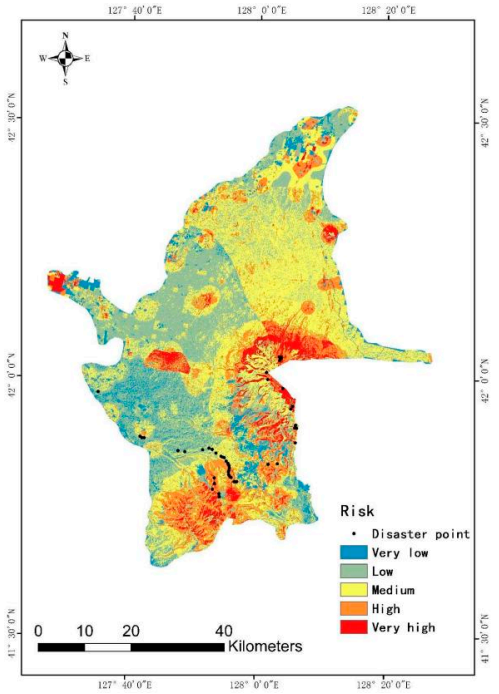


**Figure 10.** Earthquake landslide disaster risk maps.

### *5.5. Result Verification*

The ROC curve is a means to verify the accuracy of geological disaster susceptibility evaluation. The area under the ROC curve (AUC) ranged from 0.5 to 1, and higher values indicated better prediction ability of the model. The AUC value of less than 0.7 indicated poor prediction effect, 0.7–0.8 indicated moderate prediction effect, 0.8–0.9 indicated good prediction effect, and above 0.9 indicated very good prediction effect [52]. In the ROC curve, the true positive rate represents the proportion of correctly predicted positive samples (disaster hidden danger points) in the true positive samples, and the false positive rate represents the proportion of negative samples (non-disaster hidden danger points) in the true negative samples. Positive samples and negative samples are, respectively, evaluated in this method, which makes it a relatively balanced evaluation method [53]. Figure 11 shows the ROC curve of the risk outcome. The verification results showed that the area under the ROC curve was 0.8373, which indicated that the model predicted better.

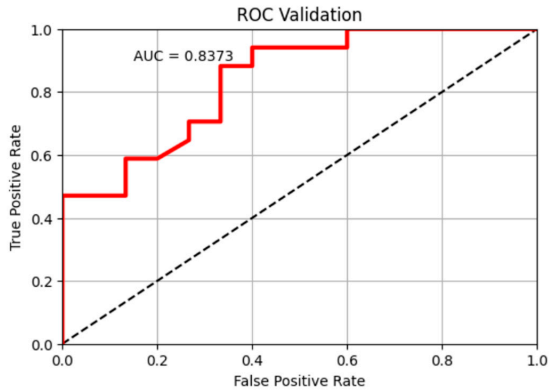


**Figure 11.** The receiver operating characteristic (ROC) curve of the risk results.

## 6. Conclusions

Previous studies mainly focused on single hazards and lacked risk evaluation of the disaster chain as a whole. This study took landslides in the context of earthquakes as the research object, and from the perspective of environmental risk, this paper selected indicators from three aspects: (i) hazard of earthquake-induced geohazard chain, (ii) exposure and vulnerability of the disaster-bearing body, and (iii) a risk assessment index system and assessment model. We carried out a risk assessment study of the earthquake-induced geohazard chain, which provided a new idea for the prevention and control study of geohazards, and was of great theoretical significance and application for the timely formulation of regional disaster prevention. It is of great theoretical significance and application value for the timely formulation of disaster prevention and mitigation policies and ecological construction.

In many studies, CF and SVM models were often used to assess the sensitivity of single hazards, and even in a small number of hazard studies, the frequency or intensity of predisposing factors were often ignored [42,43]. The Newmark model has a good performance in predicting earthquake-induced landslide events; however, the Newmark model is currently used to consider rainfall factors in earthquake landslide hazard prediction. There were a few studies, however, that used the Newmark model for predicting earthquake landslide hazards, and the coupling effect of rainfall and earthquake was found to definitely increase the probability of landslide occurrence [54]. Meanwhile, the probabilistic seismic landslide hazard evaluation method based on the Newmark displacement model suffered from the uncertainty of the evaluation model and parameters [55]. Based on the above deficiencies, this paper adopted the Newmark model to fully respond to the intensity of earthquakes as a consistent hazard factor, coupled the CF and SVM models to obtain the sensitivity, and obtained the hazard assessment results of the earthquake–landslide hazard chain based on the product of the above two. The method successfully highlighted the comprehensive understanding of the hazard chain formation mechanism and quantitatively assessed the hazard chain risk. Using this method, the risk assessment results of the Changbai Mountain earthquake–landslide hazard chain were obtained.

This paper still had some defects in the risk assessment of the disaster chain. The process of chain formation from primary to secondary disasters was complex, especially given the vulnerability of disasters due to repeated destruction of the same (or new) risk factors. Therefore, the lack of consideration of changes in vulnerability in earthquake disaster chain risk assessment was a significant drawback. Secondly, the construction, road, and other disaster carriers in the study area were more or less concentrated in one area, which had a certain impact on the exposure assessment.

**Author Contributions:** Conceptualization, K.K., Y.Z. and J.Z.; methodology, K.K.; software, K.K. and C.W.; validation, Y.Z.; formal analysis, J.Z.; investigation, K.K., Z.N. and J.W.; resources, Y.Z.; data curation, C.W. and K.K.; writing—original draft preparation, C.W.; writing—review and editing, K.K., Y.Z. and J.Z.; visualization, K.K.; supervision, Y.Z. and Y.C.; project administration, Y.Z. and Y.C. All authors have read and agreed to the published version of the manuscript.

**Funding:** This research was funded by Science and Technology Research Project of the Education Department of Jilin Province; Research on the Geological Disaster Chain Effect and the Fine Risk Early Warning Technology in the Changbai Mountain North Scenic Spot. number JJKH20210688KJ; 20220203185SF.

**Data Availability Statement:** Not applicable.

**Acknowledgments:** We would like to express our thanks to each of the authors for their contributions to this research, both in terms of data and data collection and evaluation models, as well as in computation and writing, which were the result of a joint effort.

**Conflicts of Interest:** The authors declare no conflict of interest.

## References


1. Shi, P.J. Theory and practice of disaster study. *J. Nat. Disasters* **1996**, *5*, 8–19.
2. Yin, Y.; Wang, F.; Sun, P. Landslide hazards triggered by the 2008 Wenchuan earthquake, Sichuan, China. *Landslides* **2009**, *6*, 139–152. [CrossRef]
3. Zhang, L.M.; Nadim, F.; Lacasse, S. Multi-risk assessment for landslide hazards. In Proceedings of the Pacific Rim Workshop on Innovations in Civil Infrastructure Engineering, Taipei, Taiwan, 9–11 January 2013; pp. 321–329.
4. Liu, Z.; Nadim, F.; Garcia-Aristizabal, A.; Mignan, A.; Fleming, K.; Luna, B.Q. A three-level framework for multi-risk assessment. *Georisk Assess. Manag. Risk Eng. Syst. Geohazards* **2015**, *9*, 59–74. [CrossRef]
5. Yin, Y.; Sun, P.; Zhu, J.; Yang, S. Research on catastrophic rock avalanche at Guanling, Guizhou, China. *Landslides* **2011**, *8*, 517–525. [CrossRef]
6. Zhao, L.; Li, D.; Tan, H.; Cheng, X.; Zuo, S. Characteristics of failure area and failure mechanism of a bedding rockslide in Libo County, Guizhou, China. *Landslides* **2019**, *16*, 1367–1374. [CrossRef]
7. Xu, Q.; Fan, X.; Huang, R.; Yin, Y.; Hou, S.; Dong, X.; Tang, M. A catastrophic rockslide-debris flow in Wulong, Chongqing, China in 2009: Background, characterization, and causes. *Landslides* **2010**, *7*, 75–87. [CrossRef]
8. Fan, X.; Xu, Q.; Scaringi, G.; Dai, L.; Li, W.; Dong, X.; Zhu, X.; Pei, X.; Dai, K.; Havenith, H.B. Failure mechanism and kinematics of the deadly June 24th 2017 Xinmo landslide, Maoxian, Sichuan, China. *Landslides* **2017**, *14*, 2129–2146. [CrossRef]
9. Dai, K.; Xu, Q.; Li, Z.; Tomás, R.; Fan, X.; Dong, X.; Li, W.; Zhou, Z.; Gou, J.; Ran, P. Post-disaster assessment of 2017 catastrophic Xinmo landslide (China) by spaceborne SAR interferometry. *Landslides* **2019**, *16*, 1189–1199. [CrossRef]
10. Ouyang, C.; Zhao, W.; Xu, Q.; Peng, D.; Li, W.; Wang, D.; Zhou, S.; Hou, S. Failure mechanisms and characteristics of the 2016 catastrophic rockslide at Su village, Lishui, China. *Landslides* **2018**, *15*, 1391–1400. [CrossRef]
11. Pei, R.R.; Ni, Z.Q.; Meng, Z.B.; Zhang, B.L.; Geng, Y.Y. Cause Analysis of the Secondary Mountain Disaster Chain in Wenchuan Earthquake. *Am. J. Civ. Eng.* **2017**, *5*, 414–417. [CrossRef]
12. Lyu, H.-M.; Shen, J.S.; Arulrajah, A. Assessment of Geohazards and Preventative Countermeasures Using AHP Incorporated with GIS in Lanzhou, China. *Sustainability* **2018**, *10*, 304. [CrossRef]
13. Yang, Z.H.; Lan, H.X.; Gao, X.; Li, L.P.; Meng, Y.S.; Wu, Y.M. Urgent landslide susceptibility assessment in the 2013 Lushan earthquake-impacted area, Sichuan Province, China. *Nat. Hazards* **2015**, *75*, 3467–3487. [CrossRef]
14. Han, L.; Ma, Q.; Zhang, F.; Zhang, Y.; Zhang, J.; Bao, Y.; Zhao, J. Risk Assessment of an Earthquake-Collapse-Landslide Disaster Chain by Bayesian Network and Newmark Models. *Int. J. Environ. Res. Public Health* **2019**, *16*, 3330. [CrossRef]
15. Liu, Y. *Typical Debris Flow Disaster Chain Analysis in Tibet Based on RS*; Chengdu University of Technology: Chengdu, China, 2013.
16. He, F.; Tan, S.; Liu, H. Mechanism of rainfall induced landslides in Yunnan Province using multi-scale spatiotemporalanalysis and remote sensing interpretation. *Microprocess. Microsyst.* **2022**, *90*, 104502. [CrossRef]
17. Zhu, L.; He, S.; Qin, H.; He, W.; Zhang, H.; Zhang, Y.; Jian, J.; Li, J.; Su, P. Analyzing the multi-hazard chain induced by a debris flow in Xiaojinchuan River, Sichuan, China. *Eng. Geol.* **2021**, *293*, 106280. [CrossRef]
18. Zhao, Y.; Wang, R.; Jiang, Y.; Liu, H.; Wei, Z. GIS-based logistic regression for rainfall-induced landslide susceptibilitymapping under different grid sizes in Yueqing, Southeastern China. *Eng. Geol.* **2019**, *259*, 105147. [CrossRef]
19. Tian, Y.Y.; Xu, C.; Hong, H.Y.; Zhou, Q.; Wang, D. Mapping earthquake-triggered landslide susceptibility by use of artificial neural network (ANN) models: An example of the 2013 Minxian (China) Mw 5.9 event. *Geomat. Nat. Hazards Risk* **2019**, *10*, 1–25. [CrossRef]
20. Wang, Y.; Song, C.; Lin, Q.; Li, J. Occurrence probability assessment of earthquake-triggered landslides with Newmark displacement values and logistic regression: The Wenchuan earthquake, China. *Geomorphology* **2016**, *258*, 108–119. [CrossRef]
21. Song, Y.; Gong, J.; Gao, S.; Wang, D.; Cui, T.; Li, Y.; Wei, B. Susceptibility assessment of earthquake-induced landslides using Bayesian network: A case study in Beichuan, China. *Comput. Geosci.* **2012**, *42*, 189–199. [CrossRef]
22. Gigović, L.; Pourghasemi, H.R.; Drobnjak, S.; Bai, S. Testing a new ensemble model based on SVM and random forest in forest fire susceptibility assessment and its mapping in Serbia's Tara National Park. *Forests* **2019**, *10*, 408. [CrossRef]
23. Zhou, W.; Qiu, H.; Wang, L.; Pei, Y.; Tang, B.; Ma, S.; Yang, D.; Cao, M. Combining rainfall-induced shallow landslides and subsequent debris flows for hazard chain prediction. *Catena* **2022**, *213*, 106199. [CrossRef]
24. Fan, X.; Yang, F.; Siva Subramanian, S.; Xu, Q.; Feng, Z.; Mavrouli, O.; Peng, M.; Ouyang, C.; Jansen, J.D.; Huang, R. Prediction of a multi-hazard chain by an integrated numerical simulation approach: The Baige landslide, Jinsha River, China. *Landslides* **2020**, *17*, 147–164. [CrossRef]
25. Ouyang, C.J.; He, S.M.; Tang, C.A. Numerical analysis of dynamics of debris flow over erodible beds in Wenchuan earthquake-induced area. *Eng. Geol.* **2015**, *194*, 62–72. [CrossRef]
26. Ouyang, C.J.; Zhou, K.Q.; Xu, Q.; Yin, J.H.; Peng, D.L.; Wang, D.P.; Li, W.L. Dynamic analysis and numerical modeling of the 2015 catastrophic landslide of the construction waste landfill at Guangming, Shenzhen, China. *Landslides* **2017**, *14*, 7015–7718. [CrossRef]
27. Yi, Z.H. *Analysis of Landslide Stability under Earthquake Action*; Southwest Jiaotong University: Chengdu, China, 2006.
28. Jiao, X.E. *Analysis of Landslide Stability under Seismic Action*; Southwest Jiaotong University: Chengdu, China, 2010.
29. Cattoni, E.; Salciarini, D.; Tamagnini, C. A Generalized Newmark Method for the assessment of permanent displacements of flexible retaining structures under seismic loading conditions. *Soil Dyn. Earthq. Eng.* **2019**, *117*, 221–233. [CrossRef]

30. Liu, J.M.; Shi, J.S.; Wang, T.; Wu, S.R. Seismic landslide hazard assessment in the Tianshui area, China, based on scenario earthquakes. *Bull. Eng. Geol. Environ.* **2018**, *77*, 1263–1272. [CrossRef]
31. Chousianitis, K.; Del Gaudio, V.; Kalogeras, I.; Ganas, A. Predictive model of Arias intensity and Newmark displacement for regional scale evaluation of earthquake-induced landslide hazard in Greece. *Soil Dyn. Earthq. Eng.* **2014**, *65*, 11–29. [CrossRef]
32. Del Gaudio, V.; Pierri, P.; Calcagnile, G. Analysis of seismic hazard in landslide-prone regions: Criteria and example for an area of Daunia (southern Italy). *Nat. Hazards* **2012**, *61*, 203–215. [CrossRef]
33. Sun, S.; Wang, P.; Yi, J.; Wu, C.; Wang, H.; Chen, H.; Wang, W. Types and distribution of secondary volcanic hazards in Changbaishan Tianchi and adjacent areas and their relationship with volcanic geology. *World Geol.* **2018**, *37*, 655–663.
34. Shortliffe, E.H.; Buchanan, B.G. A model of inexact reasoning in medicine. *Math. Biosci.* **1975**, *23*, 351–379. [CrossRef]
35. Heckerman, D. Probabilistic interpretations for MYCIN's certainty factors. *Mach. Intell. Pattern Recognit.* **1986**, *4*, 167–196.
36. Polat, A.; Erik, D. Debris flow susceptibility and propagation assessment in West Koyulhisar, Turkey. *J. Mt. Sci.* **2020**, *17*, 2611–2623. [CrossRef]
37. Vapnik, V. *The Nature of Statistical Learning Theory*; Springer Science & Business Media: Berlin/Heidelberg, Germany, 1999.
38. Mohammady, M.; Pourghasemi, H.R.; Amiri, M. Assessment of land subsidence susceptibility in Semnan plain (Iran): A comparison of support vector machine and weights of evidence data mining algorithms. *Nat. Hazards* **2019**, *99*, 951–971. [CrossRef]
39. Cherkassky, V. The nature of statistical learning theory. *IEEE Trans. Neural Netw.* **1997**, *8*, 1564. [CrossRef]
40. Tehrany, M.S.; Pradhan, B.; Mansor, S.; Ahmad, N. Flood susceptibility assessment using GIS-based support vector machine model with different kernel types. *Catena* **2015**, *125*, 91–101. [CrossRef]
41. Wang, H.Y.; Lai, J.F.; Yang, F.L. A review of support vector machine theory and algorithm research. *Comput. Appl. Res.* **2014**, *31*, 1281–1286.
42. Li, Y.; Mei, H.; Ren, X.; Hu, X.; Li, M. Evaluation of geological disaster susceptibility based on deterministic coefficient and support vector machine. *J. Earth Inf. Sci.* **2018**, *20*, 1699–1709.
43. Xue, Y.; Wang, Y.; Zhu, J.; Li, H.; Zhang, M. Study on sensitivity assessment of geological slope based on CF and SVM. *J. Taiyuan Univ. Technol.* **2022**, *53*, 672–681. [CrossRef]
44. Wang, T. *Research on Geological Hazard Assessment in the Hardest Hit Areas of Wenchuan Earthquake*; China Academy of Geological Sciences: Beijing, China, 2010.
45. Jibson, R.W. Regression models for estimating coseismic landslide displacement. *Eng. Geol.* **2007**, *91*, 209–218. [CrossRef]
46. Wilson, R. Predicting areal limit of earthquake-induced landsliding, evaluating eathquake hazards in the Los Angeles region-an earth-science perspective. *US Geol. Survery Prof. Pap.* **1985**, *1360*, 317–345.
47. Ding, B.; Sun, J.; Li, X.; Liu, Z.; Du, J. Research progress and discussion of the correlation between seismic intensity and ground motion parameters. *J. Earthq. Eng. Eng. Vib.* **2014**, *34*, 7–20.
48. Newmark, N.M. Effects of Earthquakes on Dams and Embankments. *Géotechnique* **1965**, *15*, 139–160. [CrossRef]
49. Du, Y.; Ge, Y.; Liang, X.; Sun, Q.; Chen, P. Study on the assessment method of the deterministic coefficient and geodetector model—Take the Anning River basin as an example. *J. Disaster Prev. Mitig. Eng.* **2022**, *42*, 664–673. [CrossRef]
50. Li, W.; Hong, T.; Xu, S.; Chen, M.; Qin, Y.; Zeng, L. Evaluation of geological disaster susceptibility in Rongjiang County based on I method and CF method. *Geol. Disaster Environ. Prot.* **2022**, *33*, 42–48.
51. Smith, R.; Kilburn, C.R.J. Forecasting eruptions after long repose intervals from accelerating rates of rock fracture: The June 1991 eruption of Mount Pinatubo, Philippines. *J. Volcanol. Geotherm. Res.* **2010**, *191*, 129–136. [CrossRef]
52. Swets, J.A. Measuring the accuracy of diagnostic systems. *Science* **1988**, *240*, 1285–1293. [CrossRef]
53. Fawcett, T. An introduction to ROC analysis. *Pattern Recognit. Lett.* **2006**, *27*, 861–874. [CrossRef]
54. Lei, Z.; Li, L.; Long, J.; Chen, J.; Yang, Y. Improvement of Newmark model based on rainfallinfiltration and prediction of seismic landslide hazard. *J. Earthq. Eng.* **2022**, *44*, 527–534. [CrossRef]
55. Zhao, N.; Ma, F.S.; Li, C.Q.; Guo, J.; Zhang, J.C. Optimization and application of parameters of probabilistic seismic landslide hazard model based on Newmark model: An example in Ludian seismic zone. *Earth Sci.* **2022**, *47*, 4401–4416.